

Finite element analysis of vertebroplasty in the osteoporotic T11L1 vertebral body: Effects of bone cement formulation

Original

Finite element analysis of vertebroplasty in the osteoporotic T11L1 vertebral body: Effects of bone cement formulation / Mondal, Subrata; Macmanus, David B.; Banchenicot, Federica; Vitalebrovarone, Chiara; Fiorilli, Sonia; Mccarthy, Helen O.; Dunne, Nicholas. - In: JOURNAL OF BIOMEDICAL MATERIALS RESEARCH. PART B, APPLIED BIOMATERIALS.. - ISSN 1552-4973. - 112:1(2024). [10.1002/jbm.b.35359]

Availability:

This version is available at: 11583/2988787 since: 2024-05-16T10:34:36Z

Publisher:

WILEY

Published

DOI:10.1002/jbm.b.35359

Terms of use:

This article is made available under terms and conditions as specified in the corresponding bibliographic description in the repository

Publisher copyright

(Article begins on next page)

RESEARCH ARTICLE

Finite element analysis of vertebroplasty in the osteoporotic T11-L1 vertebral body: Effects of bone cement formulation

Subrata Mondal¹  | David B. MacManus^{1,2} | Federica Banche-Niclot³ | Chiara Vitale-Brovarone³ | Sonia Fiorilli³ | Helen O. McCarthy⁴ | Nicholas Dunne^{1,5,6,7,8,9,10,11}

¹School of Mechanical and Manufacturing Engineering, Dublin City University, Dublin 9, Ireland

²BRAIN Lab, School of Mechanical & Materials Engineering, University College Dublin, Dublin 4, Ireland

³Department of Applied Science and Technology, Politecnico di Torino, Turin, Italy

⁴School of Pharmacy, Queen's University Belfast, Belfast, BT9 7 BL, UK

⁵Centre for Medical Engineering Research, Dublin City University, Dublin 9, Ireland

⁶Department of Mechanical and Manufacturing Engineering, School of Engineering, Trinity College Dublin, Dublin 2, Ireland

⁷Advanced Manufacturing Research Centre (I-Form), School of Mechanical and Manufacturing Engineering, Dublin City University, Dublin 9, Ireland

⁸Advanced Materials and Bioengineering Research Centre (AMBER), Trinity College Dublin, Dublin 2, Ireland

⁹Trinity Centre for Biomedical Engineering, Trinity Biomedical Sciences Institute, Trinity College Dublin, Dublin 2, Ireland

¹⁰Advanced Processing Technology Research Centre, Dublin City University, Dublin 9, Ireland

¹¹Biodesign Europe, Dublin City University, Dublin 9, Ireland

Correspondence

Nicholas Dunne, School of Mechanical and Manufacturing Engineering, Dublin City University, Dublin 9, Ireland.
Email: nicholas.dunne@dcu.ie

Funding information

European Union's Horizon 2020, Grant/Award Number: 814410

Abstract

Vertebral compression fractures are one of the most severe clinical consequences of osteoporosis and the most common fragility fracture afflicting 570 and 1070 out of 100,000 men and women worldwide, respectively. Vertebroplasty (VP), a minimally invasive surgical procedure that involves the percutaneous injection of bone cement, is one of the most efficacious methods to stabilise osteoporotic vertebral compression fractures. However, postoperative fracture has been observed in up to 30% of patients following VP. Therefore, this study aims to investigate the effect of different injectable bone cement formulations on the stress distribution within the vertebrae and intervertebral discs due to VP and consequently recommend the optimal cement formulation. To achieve this, a 3D finite element (FE) model of the T11-L1 vertebral body was developed from computed tomography scan data of the spine. Osteoporotic bone was modeled by reducing the Young's modulus by 20% in the cortical bone and 74% in cancellous bone. The FE model was subjected to different physiological movements, such as extension, flexion, bending, and compression. The osteoporotic model caused a reduction in the average von Mises stress compared with the normal model in the T12 cancellous bone and an increment in the average von Mises stress value at the T12 cortical bone. The effects of VP using different formulations of a novel injectable bone cement were modeled by replacing a region of T12 cancellous bone with the materials. Due to the injection of the bone cement at the T12 vertebra, the average von Mises stresses on cancellous bone increased and slightly decreased on the cortical bone under all loading conditions. The novel class of bone cements investigated herein demonstrated an effective restoration of stress distribution to physiological levels within treated vertebrae, which could offer a potential superior alternative for VP surgery as their anti-osteoclastogenic properties could further enhance the appeal of their fracture treatment and may contribute to improved patient recovery and long-term well-being.

KEYWORDS

finite element analysis, injectable bone cement, osteoporotic fracture, vertebra, vertebroplasty

This is an open access article under the terms of the [Creative Commons Attribution](https://creativecommons.org/licenses/by/4.0/) License, which permits use, distribution and reproduction in any medium, provided the original work is properly cited.

© 2024 The Authors. *Journal of Biomedical Materials Research Part B: Applied Biomaterials* published by Wiley Periodicals LLC.

1 | INTRODUCTION

Osteoporosis (OP) is a progressively widespread disease worldwide.¹ It is often referred to as a silent disease as bone loss, caused by the bone resorption overactivity of osteoclasts (OC), gradually occurs without evident signs and symptoms resulting in affected people often being unaware of the increased fracture risk.² OP can result in different types of fractures located in dissimilar body parts, typically occurring at the femur, forearm, pelvis, and spine vertebrae.¹ Vertebral compression fracture (VCF) is one of the most severe clinical consequences of OP and the most common fragility fracture stated in the literature.^{3,4} Based on the age- and sex-adjusted incidence, the statistics from European Prospective Osteoporosis Study Group states that VCF incidence rate of 570 and 1070 for every 100,000 people of men and women, respectively.⁵ VCFs mostly occur in the thoracolumbar junction (i.e., the spine segment from T12 to L2) with an incidence rate of 60% to 75%,⁶ whereas 30% arise in the L2 to L5 region.⁷ Vertebroplasty (VP) is a minimally invasive surgery and one of the most efficient methods to treat osteoporotic VCF in recent years.⁸ This surgery is based on the percutaneous injection of a viscous bone cement into the fractured vertebrae. The cement is normally prepared by mixing a powder phase with an appropriated volume of liquid phase. The hardening of the cement within the vertebral body allows for the restoration and stabilization of the fractured site and in turn relieves the patient's pain.^{9–12} This approach is also effective in preventing the formation of new fractures, as the bone cements should mimic the natural bone's rigidity, allowing optimal load distribution across the adjacent vertebrae, and avoiding the effects of pillaring. Nevertheless, there are still a significant number of reported cases where the treated vertebral body and adjacent vertebral body collapse following VP.^{1,13,14} Tanigawa et al.¹⁵ performed follow-up outcomes assessment on 194 patients after an average of 33 months, discovering that 33% of patients suffered fractures after VP, with 67% of these fractures occurring in the adjacent vertebrae. Surgical procedures, bone cement volume, material stiffness, filling patterns of the cement, and anti-osteoporotic treatment were identified as the potential causes for postoperative vertebral collapse.^{16–18} Furthermore, the detailed mechanisms of postoperative collapse of the treated and adjacent vertebral body are generally indistinct.¹⁹ Therefore, these causes need to be understood and rectified for the long-term efficacy of VP.

As far as bone cements currently used in clinics, polymethyl methacrylate (PMMA) based cements are the most commonly used in VP procedures.^{20,21} The clinical outcomes following PMMA VP showed enhanced stability of the vertebral body.^{20,21} However, PMMA-based inert cements lack in osteointegration and the high exothermic temperature reached during their polymerization reaction can cause necrosis of the surrounding tissue.^{22–24} Moreover, current practices demonstrated that they can cause postoperative vertebral collapse due to its excessive stiffness.^{25–32} As a valid alternative, resorbable calcium sulfate (CS)-based cements were largely used in VP due to their great biocompatibility and their ability to actively interact with the body.^{24,33} Hardening of this cement occurs spontaneously at physiological temperatures (i.e., 37°C) due to the precipitation reaction that occurs when calcium silicate hemihydrate (CSH) is combined with water, which improves the strength and the stability of the damaged vertebrae.³⁴ Since these ceramic-based cements are inherently more brittle

compared with their polymeric counterparts, composite materials obtained by the dispersion of particles within the CS matrix have been designed to overcome this limitation.³⁵ One such composite-based cement is Cerament[®], a commercially available CS-based cement that consists of 40 wt% hydroxyapatite (HA) nanoparticles. Depending on the type of particles introduced in the matrix, different properties can be conferred to the composite cement. For instance, Dadkhah et al.³⁶ introduced mesoporous bioactive glasses (MBG) particles to improve the bioactivity of CS-based cement. Moreover, several therapeutic ions can be included into the MBG composition. In the bone regeneration scenario, strontium (Sr²⁺) is widely exploited to impart pro-osteogenic features and it is currently used for the treatment of OP.³⁷

Within the framework of the H2020 GIOTTO project,² the authors optimized the formulation of an injectable, resorbable, radiopaque, and pro-osteogenic composite bone cement able to stimulate an appropriate bone remodeling response while providing the necessary stability in the treated and adjacent vertebral body.³⁸ The solid phase of this cement consists in a mixture of different powders that are α -calcium sulfate hemihydrate particles (α -CSH) chosen as resorbable matrix, enriched with commercially available zirconia nanoparticles (ZrO₂) to achieve a suitable and homogenous radiopacity throughout the material and Sr²⁺-containing MBG (Sr-MBG) nanoparticles synthesized via a sol-gel method to promote the bone remodeling process. In particular, bioactivity and pro-osteogenic effects are conferred due to the well-known HA-forming ability exhibited by MBG³⁹ and the release of Sr²⁺ ions, respectively. Furthermore, considering the OP context, anti-osteoclastogenic features were imparted to the cement by introducing a recombinant biomolecule, ICOS-Fc,⁴⁰ into the material formulation exploiting different drug delivery strategies. In particular, ICOS-Fc was encapsulated into poly (lactic-co-glycolic) acid nanoparticles (ICOS-PLGA) and covalently grafted on Sr-MBG surface (Sr-MBG-ICOS). According to these considerations, two different cement formulations were developed, resulting in different stiffness and Young's modulus values: 75CSH/20Sr-MBG/5ZrO₂ + 0.5wt% ICOS-PLGA³⁸ and 75CSH/20Sr-MBG-ICOS/5ZrO₂ + 0.5wt% ICOS-PLGA.³⁸

The aim of this study was to investigate the effect of the two developed CSH-based bone cement formulations and commercial equivalent bone cements (i.e., Cerament[®] and PMMA) on the stress distributions within the treated vertebrae following VP surgery. To study this effect, a three-dimensional (3D) finite element (FE) model was developed and used to predict the mechanical behavior of the thoracolumbar junction following VP. The following objectives of the study were to: (1) predict the load transfer through healthy and osteoporotic vertebral body models under a physiological loading environment, and (2) study the effect of the different bone cement formulations on the stress distributions within the augmented vertebrae.

2 | MATERIALS AND METHODS

2.1 | FE model development

The 3D spine model consisting of the T11-L1 vertebral body was generated using a computed tomography (CT) scan of a 60-year-old male

(516 × 516 pixels, pixels size of 0.815 mm, and slice thickness of 1 mm) obtained from the Cancer Imaging Archive Database (National Cancer Institute, National Institutes of Health, MD, USA).^{41,42} The CT images were imported into MIMICS 24.0 (Materialise, Leuven, Belgium) in digital imaging and communications in medicine (DICOM) format for manual segmentation and model generation. Manual thresholding was completed in MIMICS 24.0 (Materialise, Leuven, Belgium) to separate the cortical and cancellous layer from the T11-L1 vertebral body. The average thickness of cortical bone was retained as 0.8 mm. After the development of the T11-L1 vertebral body, the intervertebral disc (IVD) comprising the annulus fibrosus and nucleus pulposus was generated. A constant layer of thickness of 0.5 mm was extruded from the T11-L1 vertebral bone surface and the Boolean operation was performed in Rhinoceros 7.0 (Robert McNeel & Associates, WA, USA) to develop the bony end plates. All components were imported into ANSYS v 20 (ANSYS, Inc., PA, USA) for further processes such as the assignment of material properties, meshing, boundary and loading conditions, and analysis. A 10-node tetrahedral element mesh was used for the discretization process with the element length sizes lying in the range 0.2–2 mm. Five ligaments namely, anterior longitudinal ligament, posterior longitudinal ligament, ligamentum flavum, interspinous ligament, and facet capsular ligament were incorporated into the model through ANSYS v 20 (ANSYS, Inc., PA, USA) using linear spring elements. Each ligament was represented with ten parallel springs to accurately distribute the load at the ligament-bone junctions. The location and insertion point of the ligaments from existing literature were used.^{43,44} The outline for the development of the T11-L1 FE model is shown in Figure 1.

As OP leads to a reduction of bone quality and consequently its Young's modulus and density, the bone properties for the osteoporotic T12 vertebral body model were modified according to Wang et al. and Peng et al.^{43,44} The bone tissue properties of cortical and cancellous bone of the healthy T11-L1 vertebral body, the osteoporotic T12 vertebral body, IVD, and endplates were considered linear, elastic, and isotropic and are shown in Table 1.^{43,44} The length, stiffness, Young's modulus, and Poisson's ratio values of each ligament were taken from the available literature and presented in Table 2.^{43,44}

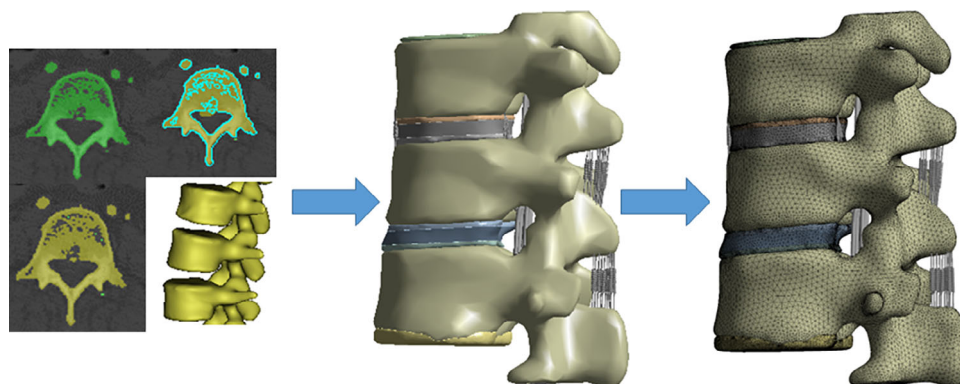


FIGURE 1 The generation of the T11-L1 vertebra finite element model from computed tomography data.

2.2 | Boundary and loading conditions

The FE model was subjected to five loading conditions, that is, compression, flexion, extension, left bending, and right bending, respectively (Figure 2). An axial force of 500 N was applied for the compression loading condition similar to a previous study.⁴³ A moment of 10 N m with a preload of 500 N (to simulate the weight of the upper body segment) was applied for the flexion, extension, and left/right bending respectively similar to a previous study.⁴³ The direction of the applied moment and axial compression force is shown in Figure 2. The bottom surface of the L1 vertebra was fully constrained.⁴³

2.3 | Overview of bone cement

The injectable, resorbable, radiopaque, pro-osteogenic, and anti-osteoclastogenic bone cement developed in the frame of the H2020 GIOTTO project² aims to treat VCF and to stimulate an appropriate bone remodeling response for effective healing. The cement was prepared by mixing a dry phase, consisting of a mixture of powders, with an aqueous phase to obtain a paste-like material that can be directly injected into the fractured site. The powder component consisted of α -CSH as a resorbable matrix, enriched with Sr-MBG and ZrO_2

TABLE 1 Material property data of the bone, intervertebral discs, and endplates.^{43,44}

| Component | Young's modulus (MPa) | Poisson's ratio (ν) |
|------------------------------|-----------------------|---------------------------|
| Healthy cortical Bone | 10,000 | 0.3 |
| Osteoporotic cortical bone | 8,040 | 0.3 |
| Healthy cancellous bone | 132 | 0.2 |
| Osteoporotic cancellous bone | 34 | 0.2 |
| Endplate | 23.8 | 0.4 |
| Fibrous annulus | 5 | 0.45 |
| Nucleus pulposus | 9 | 0.4 |

| Ligaments | Young's modulus (MPa) | Poisson's ratio (ν) | Stiffness (N/mm) |
|---------------------------------|-----------------------|---------------------------|------------------|
| Anterior longitudinal ligament | 8 | 0.28 | 45.2 |
| Posterior longitudinal ligament | 10 | 0.45 | 26.49 |
| Ligamentum Flavum | 20 | 0.45 | 43.71 |
| Interspinous ligament | 12 | 0.45 | 35.5 |
| Facet capsular ligament | 7 | 0.3 | 36.9 |

TABLE 2 Material properties and stiffness of the ligaments.^{43–46}

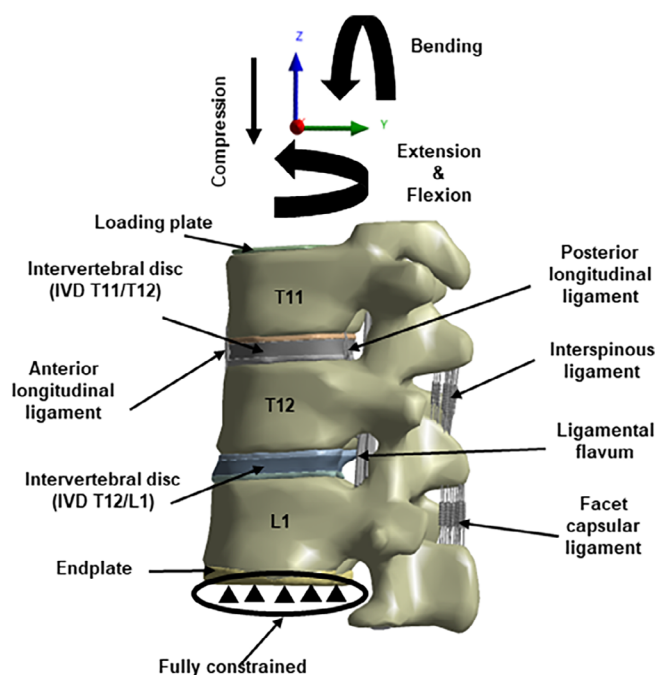


FIGURE 2 The T11-L1 vertebra model with ligaments, and the applied loading and boundary conditions.

nanoparticles to impart, respectively, bioactivity and pro-osteogenic effects as well as radiopacity. Moreover, with the purpose of retarding the resorption activity of OC that are characteristic of OP, the anti-osteoclastic biomolecule (ICOS-Fc) was included in the cement formulation following two different strategies. Specifically, polymeric nanoparticles containing ICOS-Fc (i.e., ICOS-PLGA) and Sr-MBG with ICOS-Fc covalently grafted on their surface (i.e., Sr-MBG-ICOS) were dispersed in the cement matrix.

In this study, the effect of two cement formulations on the stress distributions within the treated vertebrae following VP surgery were investigated and compared to the effect of two commercially available equivalent bone cements (i.e., PMMA and Cerament®). The examined materials were named Cement 1 (PMMA), Cement 2 (Cerament®), and Cement 3 (formulation 75CSH/20Sr-MBG/5ZrO₂ + 0.5wt% ICOS-PLGA) and Cement 4 (formulation 75CSH/20Sr-MBG-ICOS/5ZrO₂ + 0.5wt% ICOS-PLGA). Four different FE material models were developed based on the injection of the four different cement formulations. A virtual positioning and operation using Rhinoceros 7.0 (Robert McNeel & Associates, WA, USA) was performed to place the bone cements within the T12 vertebral body representing the vertebral environment postimplantation. The position of the bone cement was identical for all four cement models.

The placement of the bone cement was determined based on previous work by Peng et al.⁴³ Young's moduli of $1,076.90 \pm 358.70$, 862.40 ± 412.92 , 729.62 ± 26.17 MPa were measured experimentally for Cement 2, Cement 3, and Cement 4, respectively. The elastic modulus was characterized through mechanical testing of the cement.³⁸ Uniaxial compression mechanical testing was conducted in accordance with standard ISO 5833-2002 on cylindrical specimen (6×12 mm, $D \times H$) using the Zwick Z5 Testing Machine (Zwick Roell, Leominster, UK) fitted with a 5 kN load cell.³⁸ In particular, the samples were tested at two different time points, after 24 h (under wet conditions) and 7 days (under dry conditions) from the end of mixing to assess the initial and posthydrated mechanical behavior of the cement. Both types were placed in an incubator at $37 \pm 1^\circ\text{C}$ under 100% (wet) and 0% (dry) humidity conditions. A compressive load was applied at a rate of displacement of 1 mm/min using a preload of 5 N at a room temperature of $23 \pm 1^\circ\text{C}$. Prior to the mechanical testing, the diameter of each specimen was measured. Each specimen was tested to failure to determine the compressive strength (i.e., maximum failure load/cross-sectional area of specimen).³⁸ During this test, a load-deformation curve was obtained. Stress-strain curve was determined by using load-deflection data. After obtaining the stress-strain curve, the Young's Modulus was determined for the novel cement composition. Based on previous studies, the Young's modulus of Cement 1 (PMMA) was taken to be 2,000 MPa.^{22,47} The Poisson's ratio was assumed to be 0.3 for the all cement models, which is comparable to PMMA-based bone cement.⁴⁷ The 3D FE model of the T12-L1 vertebral body with the bone cement implantation is shown in Figure 3.

2.4 | Verification of the FE model

A mesh convergence study was performed to verify the model independency on element size. Four meshes of different element sizes and lengths were produced. A sensitivity study was performed based on the von Mises stress distribution in the T11-L1 cortical and cancellous bone. The four meshes had an increasing number of elements: Mesh 1 = 85,867; Mesh 2 = 187,921; Mesh 3 = 265,353; and Mesh 4 = 467,822 elements. The mesh element numbers were increased until the difference in the von Mises stress distribution between meshes was less than 1%. The difference between Mesh 3 and Mesh 4 showed a significant reduction in the deviation of equivalent stresses in the range of 0.1%–1%. Consequently, Mesh 3 consisting of 265,353 elements was sufficient for accurate computational modeling.

2.5 | Validation of the FE model

The present established FE model was validated with the previous postmortem human subjects (PMHS) test data using same boundary

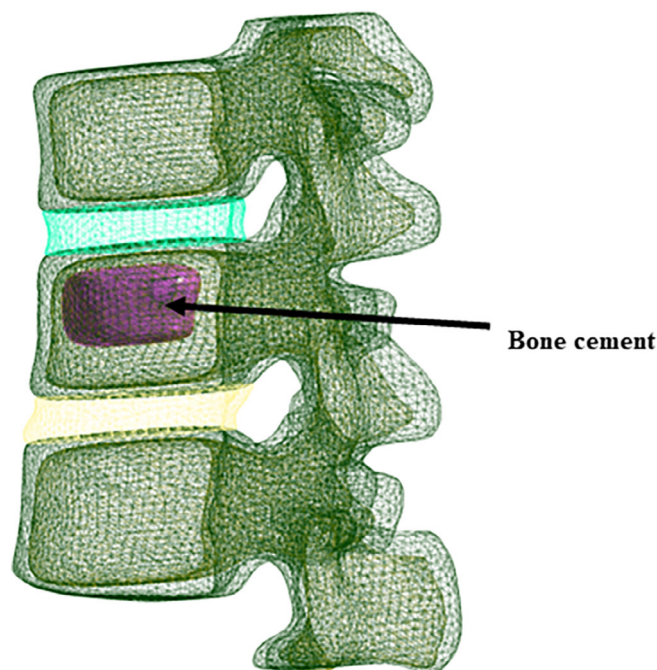


FIGURE 3 3D model of the T11-L1 vertebra with insertion of bone cement.

and loading conditions.⁴⁸ The validation of the model was done considering the range of motion (ROM) under various loading conditions. The ROM for flexion, extension, axial rotation, and lateral bending was found 1.7°, 1.8°, 1.3°, and 2.5°, respectively, at level T11-T12 and 2.1°, 2.6°, 0.8°, and 2.7°, respectively, at level T12-L1 in the present FE model, which were well within the range of previous PMHS data. The previous PMHS data reported that average \pm SD flexion, extension, axial rotation, and lateral bending ranges of motion to one side were $2.7 \pm 1.3^\circ$, $2.4 \pm 1.3^\circ$, $1.8 \pm 0.7^\circ$, and $3.5 \pm 1.1^\circ$, respectively at level T11-T12. Whereas, the ROM at T12-L1 were $2.9 \pm 1.4^\circ$, $3.9 \pm 1.4^\circ$, $1.2 \pm 0.7^\circ$, and $3.7 \pm 1.1^\circ$, respectively. The present ROMs of the established FE model were well verified and validated with the previous results.⁴⁸

3 | RESULTS

3.1 | Stress and strain distributions in the thoracolumbar junction

The results from the FE analysis of the T11-L1 spine model, corresponding to different loading conditions, are presented sequentially. The FE model was subjected to five loading conditions and the corresponding von Mises stress and strain contour plots for cortical bone were determined (Figure 4). The extension loading condition predicted the maximum stress and strain values followed by the flexion, left bending, right bending, and compression. In the case of simple

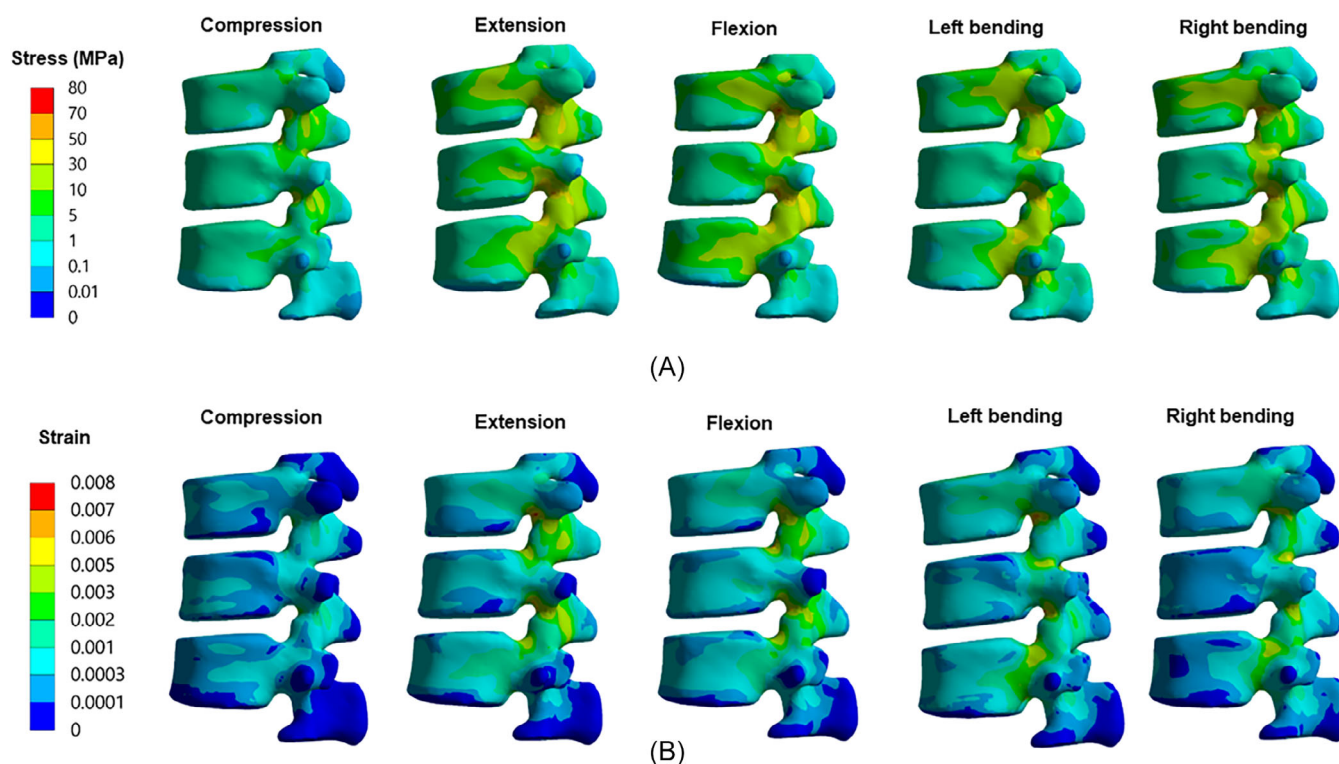


FIGURE 4 (A) von Mises stress distribution at the T11-L1 cortical vertebra, and (B) von Mises strain distribution at the T11-L1 cortical vertebra for all five loading conditions.

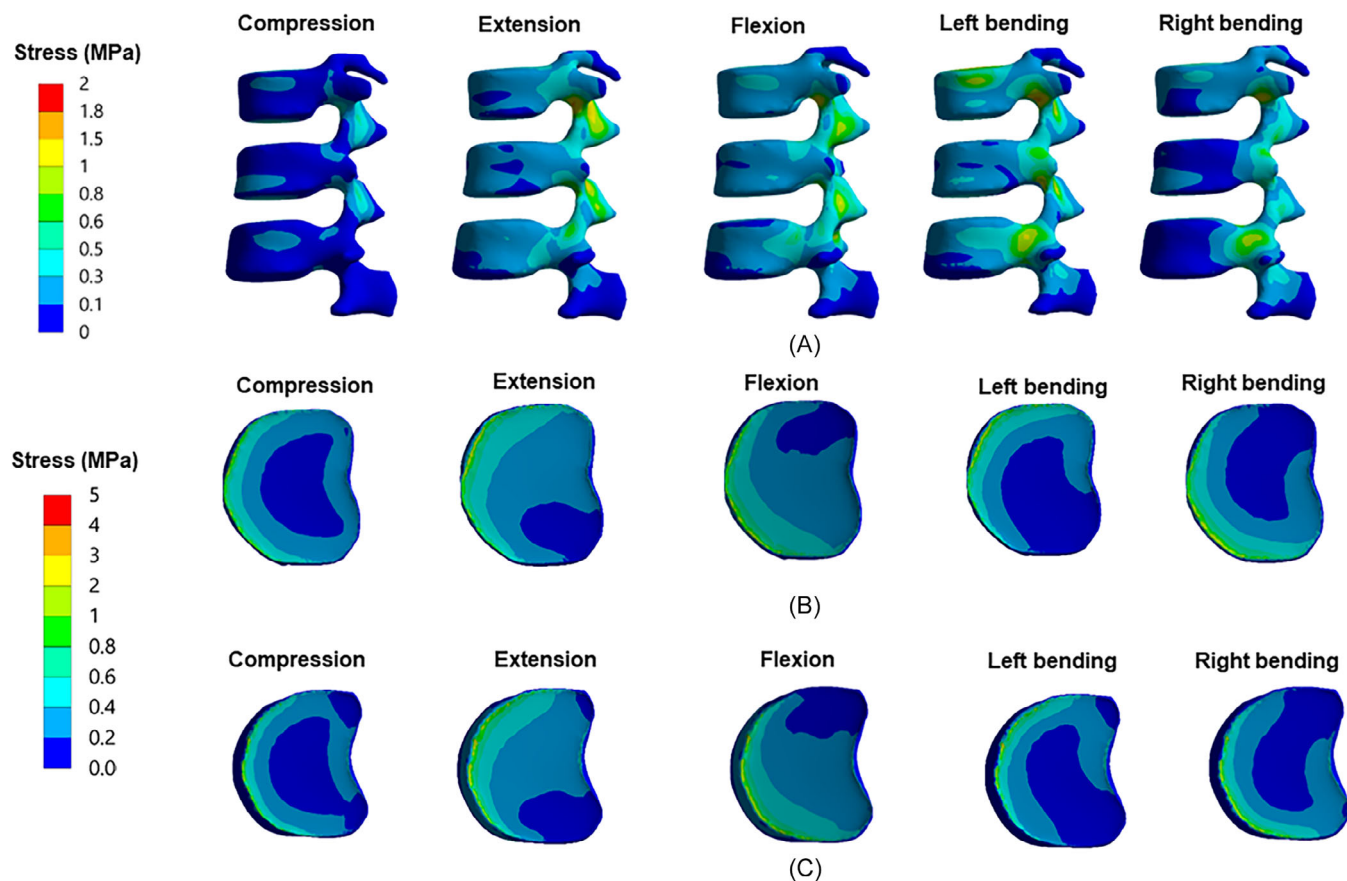


FIGURE 5 (A) von Mises stress distribution at the T11-L1 cancellous vertebrae, (B) von Mises stress distribution at the T11-T12 IVD, and (C) von Mises stress distribution at the T12-L1 IVD for all the five loading conditions.

compression, the peak value of von Mises stress and strain were predicted to be 41.85 MPa and 0.42% in the cortical bone, respectively. Whereas for extension, the peak von Mises stress and strain in the cortical bone were predicted to be 78.43 MPa and 0.79%, respectively. The equivalent stress distributions, corresponding to all the five load cases, for the T11-L1 cancellous vertebrae and IVDs (T11-T12 IVD, and T12-L1 IVD) are shown in Figure 5. Similar to the cortical bone, the highest stress value in the cancellous vertebrae was observed for the extension loading condition followed by the flexion, left bending, right bending, and compression conditions. The peak von Mises stress value in the cancellous bone was predicted to be 1.65 MPa for extension and 0.78 MPa for compression loading. The peak values in T11-T12 IVD and T12-L1 IVD were predicted to be 2.75 MPa and 4.70 MPa, respectively, in the compression loading case. Whereas for extension, the maximum stress was 2.89 MPa and 5 MPa in T11-T12 IVD and T12-L1 IVD respectively.

3.2 | Effect of bone cement on the stress distributions

The average von Mises stress values of healthy and osteoporotic bone, and after the bone cement injection were measured in the

cortical bone (T12 vertebral body) with the results for all five loading conditions presented in Figure 6. The osteoporotic FE model showed an increase in the average von Mises stress value in the cortical bone for all loading conditions compared with the healthy model. The difference in average von Mises stress values between the healthy and osteoporotic models in the T12 cortical bone was predicted to be 22.02%, 8.73%, 8.74%, 16.54%, and 18.65% for compression, extension, flexion, left bending, and right bending, respectively. A marked reduction in average von Mises stress was found following bone cement injection into the T12 vertebra compared with the osteoporotic model without cement. The average stress value at the T12 cortical bone approached that of the healthy model following the placement of the bone cement. The percentage differences in the average stress values between the healthy and Cement 1 models were predicted to be 2.87%, 1.40%, 1.36%, 7.37%, and 1.27% for compression, extension, flexion, left bending, and right bending, respectively. However, there were only negligible differences in stress distributions patterns in the cortical bone for all the four cement models subjected to physiological loading (Figure S1).

The average von Mises stress in the cancellous bone for healthy, osteoporotic, and bone cement FE models subjected to all five loading conditions were also determined (Figure 7). Contrary to what was observed in cortical bone, a decrease in the average von Mises stress

FIGURE 6 Average von Mises stress distribution in the T12 cortical bone under the five physiological loading conditions.

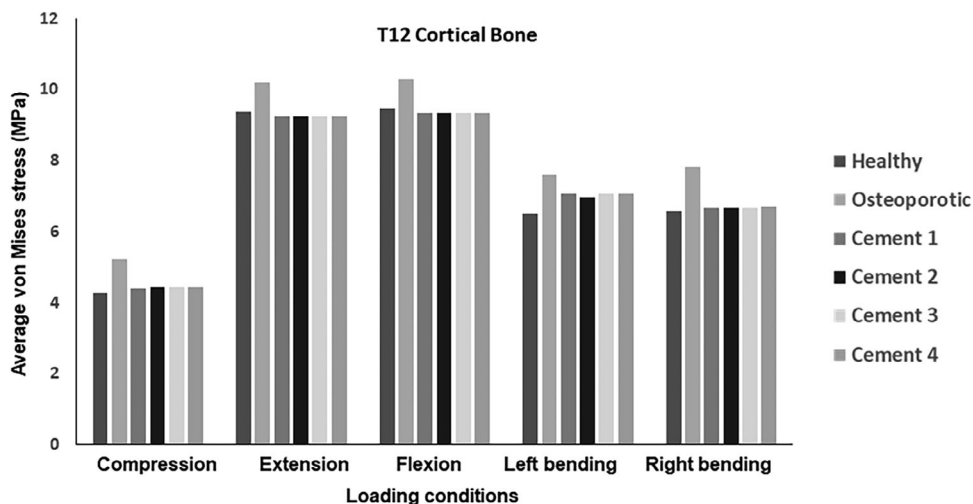


FIGURE 7 Average von Mises stress distribution in the T12 cancellous bone under the five physiological loading conditions.

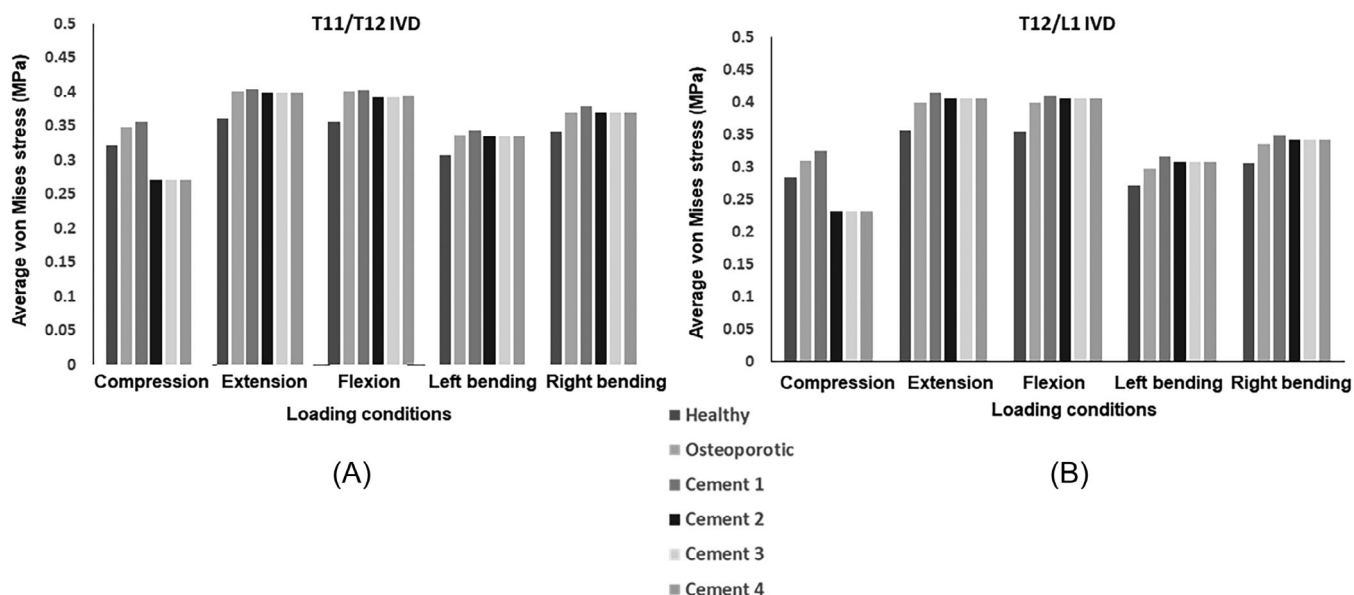
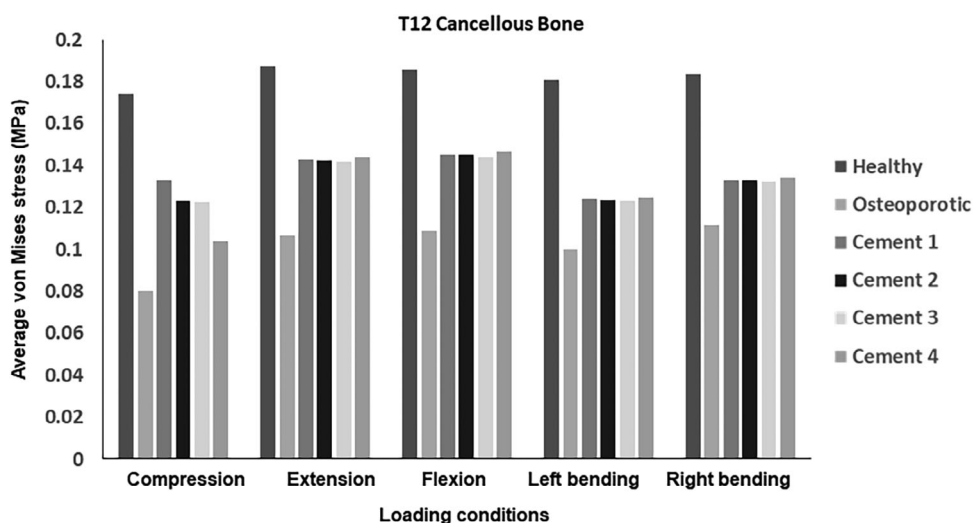


FIGURE 8 (A) Average von Mises stress distribution in the T11-T12 IVD, and (B) average von Mises stress distribution in the T12-L1 IVD under the five physiological loading conditions.

was observed for the osteoporotic FE model in the cancellous bone compared with the healthy bone (Figure 7). Furthermore, an increase in the average von Mises stress in the T12 cancellous bone was found due to the implantation of bone cements. The average von Mises stress values in the T12 cancellous bone for all the bone cement models were found to be very close to the healthy T12 cancellous bone. However, only negligible differences in the average von Mises stress were observed when a comparison was made across the four cement models (Figure S2).

Concerning the FE simulations performed in the IVD, the osteoporotic vertebral body caused the increase in average von Mises stress at the T11-T12 IVD and T12-L1 IVD when compared with the healthy model (Figure 8). Following bone cement injection into the T12 vertebral body, the average von Mises stress value decreased in the T11-T12 IVD, while a negligible increase in average von Mises stress was observed in the T12-L1 IVD for Cements 2–4. However, Cement 1, exhibited a negligible increase in stress value in both the T11-T12 IVD and T12-L1 IVD. Like the cortical and cancellous bone, no significant differences in average von Mises stresses and stress distribution patterns were observed across the four cement models (Figure S3). However, as depicted in Figure 9, the peak von Mises stress under the five physiological loading conditions was different across the four material models investigated. As expected, the peak von Mises stress was found to be greatest in Cement 1 followed by Cement 2, Cement 3, and Cement 4 for all loading conditions. The maximum stress value for all investigated Cement types was observed under the flexion loading condition, followed by extension, left bending, right bending, and compression conditions. Specifically, under flexion loading, the maximum stress values were predicted to be 9.06, 6.59, 6.39, and 4.87 MPa for Cement 1, Cement 2, Cement 3, and Cement 4, respectively. Conversely, under compression loading, the maximum stress values for Cement 1, Cement 2, Cement 3, and

Cement 4 were predicted to be 3.11, 2.23, 2.17, and 1.64 MPa, respectively (Figure 9).

4 | DISCUSSION

VCF can occur due to an osteoporotic-induced decrease in bone strength and bone quality.⁴⁹ VP is an efficient minimally invasive surgical procedure that has been widely used to treat patients suffering from VCF.⁴⁹ Previous reports suggested that injectable PMMA-based bone cements are suspected to be a potential risk factor for postoperative vertebral collapse due to its excessive stiffness.^{24–27,50} Thus, a novel resorbable composite CS-based bone cement was introduced for the VP procedure to stabilize the osteoporotic VCF alongside stimulating bone regeneration. The presented study aimed to develop a 3D FE model of the T11-L1 spine unit and investigate the effect of different bone cement formulations on the stress distributions in the treated vertebrae post VP.

Initially, the healthy T11-L1 FE model was assessed under different physiological movements to gain insights into the normal biomechanical behavior of the thoracolumbar vertebra (Figure 2). It is well established that realistic physiological loading and boundary conditions play a critical role in the stress and strain distributions in the spinal unit.^{51–55} The bulk of the load was transferred through the cortical bone of the T11-L1 vertebra, which corroborates earlier findings that show load distribution in the cortical and cancellous bone of the spinal model for different movements.^{51,52} The extension loading condition showed the highest von Mises stress in the cortical and cancellous T11-L1 bone followed by flexion, left bending, right bending, and compression loading conditions. Previous studies reported the highest stresses were observed in the T11-L1 cortical and cancellous bone under the extension loading condition, which is in agreement with our

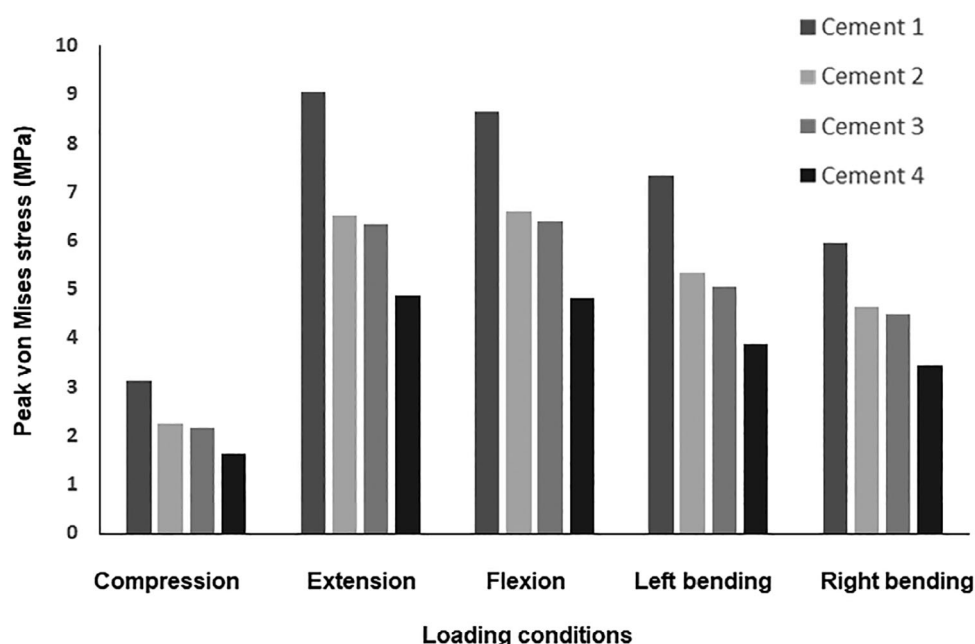


FIGURE 9 Peak von Mises stress for the four-bone cement formulations for all five loading conditions.

results.⁴³ The location of the peak von Mises stress and stress distribution patterns in the cortical, cancellous, and IVDs were found to be different for all loading conditions (Figures 4 and 5) and followed similar trends to previously reported studies.^{43,44} The osteoporotic FE model predicted a reduction in the average von Mises stress values in the T12 cancellous bone. Whereas the average von Mises stress value at the T12 cortical bone was increased. The osteoporotic vertebral body also led to an increase in the average von Mises stress value in the T11-T12 IVD and T12-L1 IVD. This stress behavior can be explained by the reduced density and increased porosity of cortical bone in OP, as it becomes weaker and more susceptible to fractures.⁵⁶ However, cancellous bone experiences greater loss in connectivity and trabecular structure.⁵⁷ The reduced trabecular network makes cancellous bone less capable of transmitting and distributing stress.⁵⁸ As a result, when external forces are applied to the spine, the stress in the cancellous bone decreases because it is less able to bear the load and distribute the stress across its network of trabeculae. Therefore, we observe increased stress values in the cortical bone.

Previous findings have highlighted that certain choices in bone cement treatment (e.g., surgical procedures, bone cement volume, material stiffness, filling patterns of the cement, and OP severity) as potential risk factors for recompression of osteoporotic spinal compression fracture. Accumulating evidence has critically linked the likelihood of vertebral body re-collapse in individuals who have undergone VP to the Young's modulus of the bone cement. An in vitro biomechanical study by Boger et al.²⁸ demonstrated that enhanced functional spine units exhibit better failure strength when utilizing a low-modulus PMMA cement than with conventional PMMA cement. In addition, several 3D FE studies on osteoporotic models have indicated that high bone cement stiffness can increase the risk of neighboring vertebral fractures postVP.³¹ However, Kim et al.²⁹ contradicted these findings, suggesting that changes in vertebral stress resulting from variations in the Young's modulus of bone cement might be negligible.²⁹ Moreover, Pneumatics et al.³⁰ reported no statistical significant changes in the compressive failure load between vertebral bodies with and without augmentation. According to our findings, the average von Mises stress of the cancellous bone of cemented vertebra gradually increased with higher Young's modulus of the bone cement under various loading conditions. This increase in local cancellous bone stress, attributed to the high Young's modulus and intensity of bone cement in the active state, may lead to vertebral body fractures.⁵⁹ Therefore, it may be more therapeutic to use a bone cement with a lower Young's modulus to prevent postoperative vertebral body fractures.⁶⁰ Considering these factors, the present study developed a FE model to investigate the effects of two novel cement formulations for VP with Young's modulus values lower than the commercially available bone cements (i.e., PMMA and Cerament®). To the best of the authors' knowledge, these novel injectable resorbable composite cements, uniquely combining pro-osteogenic and anti-osteoclastogenic features, has been designed for stabilizing and treating vertebral body fractures. Notably, these new formulations exhibit lower Young's modulus values compared with the commercially available bone cements (PMMA and Cerament®).³⁸

Bone cements are commonly implanted into the T12 vertebral body to stabilize and restore the stress distributions within the cortical and cancellous bone of the vertebra, and IVDs back to normal (healthy) values. In this study, FE models of the healthy, osteoporotic, and osteoporotic post VP models were created to investigate the biomechanical effects of novel CS-based bone cements for potential use during the VP surgical procedure and compared with a commercial reference (Cerament® and PMMA).² For the osteoporotic-treated model, a slight reduction in the average von Mises stresses was found in the T12 cortical bone when compared with the osteoporotic model (Figure 6), while an increase in the average von Mises stresses was observed in the T12 cancellous bone (Figure 7). The stress distribution in the T12 cortical and cancellous bone regions for the bone cement models matched closely to the stress distributions in the healthy model. Based on these findings, the restoration of the stress and strain distributions in the cortical and cancellous bone regions of the T12 vertebral body post-injection of the novel bone cements may improve bone quality and fracture strength.^{43,44} Simultaneously, the decrease in the average von Mises stresses in the T11-T12 IVD due to bone cement injection (Cement 2 and Cement 3) was observed, further reducing the risk of fracture in the adjacent vertebrae. Cement 1 showed slight better stress distributions when compared with Cement 2, Cement 3, and Cement 4. This is due to its higher Young's modulus of Cement 1 (2,000 MPa) compared with that of Cement 2 (1,076.90 ± 358.70 MPa), Cement 3 (862.40 ± 412.92 MPa), and Cement 4 (729.62 ± 26.17 MPa). However, there were only negligible differences in the average von Mises stresses and stress distribution patterns in the T12 cortical, cancellous, and IVD region observed for all the cement formulations. Taking together, the present study suggests that the novel formulations of CS-based bone cements, developed as part of the H2020 GIOTTO project, could present an interesting alternative to restore the stress distributions in the augmented vertebral body as well as reduce the occurrence of osteoporotic fractures in adjacent vertebrae when compared with commercially available bone cement (Cerament® and PMMA) due to their many features, one of which includes anti-osteoclastogenic characteristics.

4.1 | Limitations

Our FE model had some limitations and assumptions, which should be noted and will be addressed in future work. First, no soft tissues (e.g., skin, muscle, etc.) were considered in the current model. In line with previous work, it was assumed that the material properties of soft tissues are orders of magnitude less than those of bone,^{43,44,61,62} and that they do not have a significant effect on the stress distribution within the T11-L1 vertebral body. Second, our model of the T11-L1 vertebral body is based on a single CT scan dataset that might be beneficial for qualitative assessment of the load transfer. However, for quantitative evaluation of the load transfer applicable to a specific demographic, a morphologically averaged model of the T11-L1 vertebral body bone developed from CT scans of multiple persons is needed.⁶¹⁻⁶⁵ This is due to subject-specific morphological variability

due to sex, age, and other biological factors and might be effective for a more complete understanding of the load transfer through the T11-L1 vertebral FE model.^{66–68} Third, cancellous bone was assigned with the constant, isotropic, linear, and homogenous material properties. Whereas, the material property of cancellous bone is linear, anisotropic, and heterogeneous.^{58,69,70} However, based on previous work reported in the literature the isotropic, linear, and homogenous material properties assumption is sufficient for our modeling purposes.^{71–78} While it is true that incorporating material inhomogeneity could influence stress distribution and transmission at the bone trabeculae level,⁷⁹ for the purposes of this work, the focus was on macroscale stress changes pre and post VP using cements with varying Young's modulus values. Therefore, employing homogeneous properties was deemed sufficient. However, the FE models' biofidelity may be improved by considering the heterogeneous, anisotropic, and viscoelastic properties of cancellous bone.⁷⁶ An additional improvement to the FE model could involve incorporating the viscoelastic properties of cancellous bone, enabling a more accurate representation of its the time-dependent mechanical response under loading conditions, which could provide a more accurate representation of its mechanical response. Meanwhile, all cement material models assumed a Poisson ratio of 0.3, which aligns with values reported in the literature.^{43,44} The study focussed solely on testing under static loading conditions. However, further insights into the long-term performance of the bone cement could be gained by applying dynamic loading simulations, an aspect that will be explored in future studies. By pursuing these research directions, a more comprehensive understanding of vertebral body biomechanics and load transfer can be achieved, potentially leading to improved clinical applications and patient-specific analyses.

5 | CONCLUSIONS

A 3D FE model of the T11-L1 vertebra (including ligaments, end plates, IVDs, physiological boundary and loading conditions, and a biofidelic material property distribution) was developed to evaluate the mechanical performance of new bone cement formulations for VP surgery. The results confirm that the novel formulations of CSH-based bone cements, developed as part of the H2020 GIOTTO project, are a mechanically viable alternative to existing commercial products and are capable of restoring the loadbearing function in the augmented T11-L1 vertebral body. Further, these novel cement formulations have the advantage of containing anti-osteoclastogenic molecules capable of reducing the occurrence of osteoporotic fractures in adjacent vertebrae when compared with commercially available bone cements (PMMA and Cerament®).

ACKNOWLEDGMENTS

This study has received funding from the European Union's Horizon 2020 - Research and Innovation program under grant agreement number 814410 (GIOTTO <https://www.giotto-project.eu/>). Additionally, the CT data used in this study were generated by the National Cancer Institute Clinical Proteomic Tumor Analysis Consortium (CPTAC). Open access funding provided by IReL.

CONFLICT OF INTEREST STATEMENT

The authors declare no conflicts of interest.

DATA AVAILABILITY STATEMENT

The data that support the findings of this study are available from the corresponding author upon reasonable request.

ORCID

Subrata Mondal  <https://orcid.org/0000-0002-0702-8474>

REFERENCES

- Chen LH, Hsieh MK, Liao JC, et al. Repeated percutaneous vertebroplasty for refracture of cemented vertebrae. *Arch Orthop Trauma Surg.* 2011;131(7):927-933. doi:10.1007/s00402-010-1236-7
- Active aGelng and osteoporosis: the next challenge for smart nano-biOmaterials and 3D technologies. <https://www.giotto-project.eu/>
- Kutsal FY, Ergani GOE. Vertebral compression fractures: still an unpredictable aspect of osteoporosis. *Turk J Med Sci.* 2021;51:393-399. doi:10.3906/sag-2005-315
- Savage JW, Schroeder GD, Anderson PA. Vertebroplasty and kyphoplasty for the treatment of osteoporotic vertebral compression fractures. *J Am Acad Orthop Surg.* 2014;22(10):653-664. doi:10.1016/j.spinee.2009.01.003
- Kim HJ, Park S, Park SH, et al. Prevalence of frailty in patients with osteoporotic vertebral compression fracture and its association with numbers of fractures. *Yonsei Med J.* 2018;59(2):317-324. doi:10.3349/yymj.2018.59.2.317
- Donnelly CJ, DiPompeo CM, Varacallo M. Vertebral compression fractures. *StatPearls.* StatPearls Publishing; 2022 February 12, 2022. <https://www.ncbi.nlm.nih.gov/books/NBK448171/>
- Svedbom A, Hernlund E, Ivergård M, Compston J, et al. Osteoporosis in the European Union: a compendium of country-specific reports. *Arch Osteoporos.* 2013;8(1):137. doi:10.1007/s11657-013-0137-0
- Jay B, Ahn SH. Vertebroplasty. *Semin Interv Radiol.* 2013;30(3):297-306. doi:10.1055/s-0033-1353483
- Mehbod A, Aunoble S, Huec JCL. Vertebroplasty for osteoporotic spine fracture: prevention and treatment. *Eur Spine J.* 2003;12:155-162. doi:10.1007/s00586-003-0607-y
- Clark W, Bird P, Diamond T, Gonski P. Vertebroplasty for acute painful osteoporotic fractures (VAPOUR): study protocol for a randomized controlled trial. *Trials.* 2015;16:159. doi:10.1186/s13063-015-0671-8
- Rosenbaum BP, Kshetry VR, Kelly ML, Mroz TE, Weil RJ. Trends in inpatient vertebroplasty and kyphoplasty volume in the United States, 2005-2011: assessing the impact of randomized controlled trials. *Clin Spine Surg.* 2017;30(3):276-282. doi:10.1097/bsd.0000000000000207
- Kan SL, Yuan ZF, Chen LX, Sun JC, Ning GZ, Feng SQ. Which is best for osteoporotic vertebral compression fractures: balloon kyphoplasty, percutaneous vertebroplasty or non-surgical treatment? A study protocol for a Bayesian network meta-analysis. *BMJ Open.* 2017;7(1):012937. doi:10.1136/bmjopen-2016-012937
- Uppin AA, Hirsch JA, Centenera LV, Pfiefer BA, Pazianos AG, Choi IS. Occurrence of new vertebral body fracture after percutaneous vertebroplasty in patients with osteoporosis. *Radiology.* 2003;226(1):119-124. doi:10.1148/radiol.2261011911
- Zhang L, Wang Q, Wang L, Shen J, Zhang Q, Sun C. Bone cement distribution in the vertebral body affects chances of recompression after percutaneous vertebroplasty treatment in elderly patients with osteoporotic vertebral compression fractures. *Clin Interv Aging.* 2017;12:431-436. doi:10.2147/CIA.S113240
- Tanigawa N, Kariya S, Komemushi A, et al. Percutaneous vertebroplasty for osteoporotic compression fractures: long-term evaluation of the

- technical and clinical outcomes. *AJR Am J Roentgenol*. 2011;196:1415-1418. <https://www.ajronline.org/doi/epdf/10.2214/AJR.10.5586>
16. Lin WC, Lee YC, Ch L, et al. Refractures in cemented vertebrae after percutaneous vertebroplasty: a retrospective analysis. *Eur Spine J*. 2008;17(4):592-599. doi:10.1007/s00586-007-0564-y
 17. Ha KY, Kim YH. Risk factors affecting progressive collapse of acute osteoporotic spinal fractures. *Osteoporos Int*. 2013;24(4):1207-1213. doi:10.1007/s00198-012-2065-z
 18. Rho YJ, Choe WJ, Chun YI. Risk factors predicting the new symptomatic vertebral compression fractures after percutaneous vertebroplasty or kyphoplasty. *Eur Spine J*. 2012;21(5):905-911. doi:10.1007/s00586-011-2099-5
 19. Nouda S, Tomita S, Kin A, Kawahara K, Kinoshita M. Adjacent vertebral body fracture following vertebroplasty with polymethylmethacrylate or calcium phosphate cement: biomechanical evaluation of the cadaveric spine. *Spine*. 2009;34(24):2613-2618. doi:10.1097/brs.0b013e3181abc150
 20. He Z, Zhai Q, Hu M, et al. Bone cements for percutaneous vertebroplasty and balloon kyphoplasty: current status and future developments. *J Orthop Translat*. 2015;3(1):1-11. doi:10.1016/j.jot.2014.11.002
 21. Bae H, Hatten HP Jr, Linovitz R, et al. A prospective randomized FDA-IDE trial comparing Cortoss with PMMA for vertebroplasty: a comparative effectiveness research study with 24-month follow-up. *Spine*. 2012;37(7):544-550. doi:10.1097/brs.0b013e31822ba50b
 22. Dunne NJ, Orr JF. Thermal characteristics of curing acrylic bone cement. *ITBM-RBM*. 2001;22(2):88-97. doi:10.1016/S1297-9562(01)90034-8
 23. Dunne N. Mechanical properties of bone cements. In Sanjukta Deb (eds) *Ortho Bone Cements*. Woodhead Publishing; 2008:233-264 <https://www.elsevier.com/books/orthopaedic-bone-cements/deb/978-1-84569-376-3>
 24. Yousefi AM. A review of calcium phosphate cements and acrylic bone cements as injectable materials for bone repair and 1038 implant fixation. *J Appl Biomater Funct Mater*. 2019;17:2280800019872594. doi:10.1177/2280800019872594
 25. Heini PF, Walchli B, Berlemann U. Percutaneous transpedicular vertebroplasty with PMMA: operative technique and early results. A prospective study for the treatment of osteoporotic compression fractures. *Eur Spine J*. 2000;9(5):445-450. doi:10.1007/s005860000182
 26. Tai CL, Lai PL, Lin WD, et al. Modification of mechanical properties, polymerization temperature, and handling time of polymethylmethacrylate cement for enhancing applicability in vertebroplasty. *Biomed Res Int*. 2016;2016:7901562. doi:10.1155/2016/7901562
 27. Hoppe S, Wangler S, Aghayev E, Gantenbein B, Boger A, Benneker LM. Reduction of cement leakage by sequential PMMA application in a vertebroplasty model. *Eur Spine J*. 2016;25(11):3450-3455. doi:10.1007/s00586-015-3920-3
 28. Boger A, Heini P, Windolf M, Schneider E. Adjacent vertebral failure after vertebroplasty: a biomechanical study of low modulus PMMA cement. *Eur Spine J*. 2007;16(12):2118-2125. doi:10.1007/s00586-007-0473-0
 29. Kim JM, Shin DA, Byun DH, Kim HS, Kim S, Kim HI. Effect of bone cement volume and stiffness on occurrences of adjacent vertebral fractures after vertebroplasty. *J Korean Neurosurg Soc*. 2012;52(5):435-440. doi:10.3340/jkns.2012.52.5.435
 30. Pneumáticos SG, Triantafyllopoulos GK, Evangelopoulos DS, Hipp JA, Heggeness MH. Effect of vertebroplasty on the compressive strength of vertebral bodies. *Spine J*. 2013;13(12):1921-1927. doi:10.1016/j.spinee.2013.06.054
 31. Cho AR, Cho SB, Lee JH, et al. Effect of augmentation material stiffness on adjacent vertebrae after osteoporotic vertebroplasty using finite element analysis with different loading methods. *Pain Physician*. 2015;18(6):1101-1110. <https://pubmed.ncbi.nlm.nih.gov/26606023/>
 32. Wijayathunga VN, Oakland RJ, Jones AC, Hall RM, Wilcox RK. Vertebroplasty: patient and treatment variations studied through parametric computational models. *Clin Biomech*. 2013;28(8):860-865. doi:10.1016/j.clinbiomech.2013.07.012
 33. Dorozhkin SV. Biocomposites and hybrid biomaterials based on calcium orthophosphates. *Biomater*. 2011;1(1):3-56. doi:10.4161/biom.1.1.16782
 34. Hand RJ. The kinetics of hydration of calcium sulphate hemihydrate: a critical comparison of the models in the literature. *Cem Concr Res*. 1994;24:885-895. doi:10.1016/0008-8846(94)90008-6
 35. O'Hara RM, Dunne NJ, Orr JF, et al. Optimisation of the mechanical and handling properties of an injectable calcium phosphate cement. *J Mater Sci Mater Med*. 2010;21(8):2299-2305. doi:10.1007/s10856-009-3977-9
 36. Dadkhah M, Pontiroli L, Fiorilli S, et al. Preparation and characterisation 1144 of an innovative injectable calcium sulphate based bone cement for vertebroplasty application. *J Mater Chem B*. 2017;5:102. <https://pubs.rsc.org/en/content/articlelanding/2017/tb/c6tb02139e-115>.
 37. Wu Q, Hu L, Yan R, et al. Strontium-incorporated bioceramic scaffolds for 1074 enhanced osteoporosis bone regeneration. *Bone Res*. 2022;10:55. doi:10.1038/s41413-022-00224-x
 38. Banche-Niclot F, Corvaglia I, Cavallera C, et al. Optimization of an injectable, resorbable, bioactive cement able to release the anti-osteoclastogenic biomolecule ICOS-Fc for the treatment of osteoporotic vertebral compression fractures. *Biomolecules*. 2023;13(1):94. doi:10.3390/biom13010094
 39. Rahaman MN, Day DE, Sonny B, et al. Bioactive glass in tissue engineering. *Acta Biomater*. 2011;7:2355-2373. doi:10.1016/j.actbio.2011.03.016
 40. Gigliotti CL, Boggio E, Clemente N, et al. ICOS-ligand triggering impairs osteoclast differentiation and function in vitro and in vivo. *J Immunol*. 2016;197:3905-3916. doi:10.4049/jimmunol.1600424
 41. National Cancer Institute Clinical Proteomic Tumor Analysis Consortium (CPTAC). Radiology Data from the Clinical Proteomic Tumor Analysis Consortium Sarcomas [CPTAC-SAR] collection [C3N-00875]. The Cancer Imaging Archive. 2018. doi:10.7937/tcia.2019.9bt23r95
 42. Clark K, Vendt B, Smith K, et al. The cancer imaging archive (TCIA): maintaining and operating a public information repository. *J Digit Imaging*. 2013;26(6):1045-1057. doi:10.1007/s10278-013-9622-7
 43. Peng Y, Du X, Huang L, et al. Optimizing bone cement stiffness for vertebroplasty through biomechanical effects analysis based on patient-specific three-dimensional finite element modeling. *Med Biol Eng Comput*. 2018;56:2137-2150. doi:10.1007/s11517-018-1844-x
 44. Wang D, Li Y, Yin H, et al. Three-dimensional finite element analysis of optimal distribution model of vertebroplasty. *Ann Palliat Med*. 2020;9(3):1062-1072. doi:10.21037/apm-20-955
 45. Erbulut DU, Zafarparandeh I, Lazoglu I, Ozer AF. Application of an asymmetric finite element model of the C2-T1 cervical spine for evaluating the role of soft tissues in stability. *Med Eng Phys*. 2014;36:915-921. doi:10.1016/j.medengphys.2014.02.020
 46. Yoganandan N, Kumaresan S, Pintar FA. Geometric and mechanical properties of human cervical spine ligaments. *J Biomech Eng*. 2000;122(6):623-629. doi:10.1115/1.1322034
 47. Buckley PJ, Orr JF, Revie IC, Breusch SJ, Dunne NJ. Fracture characteristics of acrylic bone cement-bone composites. *Proc Inst Mech Eng H*. 2003;217(6):419-427. doi:10.1243/09544110360729063
 48. Panjabi MM, Oxland TR, Yamamoto I, Crisco JJ. Mechanical behavior of the human lumbar and lumbosacral spine as shown by three-dimensional load-displacement curves. *J Bone Joint Surg Am*. 1994;76(3):413-424. doi:10.2106/00004623-199403000-00012
 49. Brodano GB, Amendola L, Martikos K, et al. Vertebroplasty: benefits are more than risks in selected and evidence-based informed patients.

- A retrospective study of 59 cases. *Eur Spine J*. 2011;20(8):1265-1271. doi:[10.1007/s00586-011-1705-x](https://doi.org/10.1007/s00586-011-1705-x)
50. Lewin S, Försth P, Persson C. Low-modulus PMMA has the potential to reduce stresses on endplates after cement discoloplasty. *J Funct Biomater*. 2022;13(1):18. doi:[10.3390/jfb13010018](https://doi.org/10.3390/jfb13010018)
 51. Talukdar RG, Mukhopadhyay KK, Dhara S, Gupta S. Numerical analysis of the mechanical behaviour of intact and implanted lumbar functional spinal units: effects of loading and boundary conditions. *Proc Inst Mech Eng H*. 2021;235(7):792-804. doi:[10.1177/09544119211008343](https://doi.org/10.1177/09544119211008343)
 52. Kang S, Park CH, Jung H, et al. Analysis of the physiological load on lumbar vertebrae in patients with osteoporosis: a finite-element study. *Sci Rep*. 2022;12:11001. doi:[10.1038/s41598-022-15241-3](https://doi.org/10.1038/s41598-022-15241-3)
 53. Newell N, Little JP, Christou A, Adams MA, Adam CJ, Masouros SD. Biomechanics of the human intervertebral disc: a review of testing techniques and results. *J Mech Behav Biomed Mater*. 2017;69:420-434. doi:[10.1016/j.jmbbm.2017.01.037](https://doi.org/10.1016/j.jmbbm.2017.01.037)
 54. Zahari SN, Latif MJA, Rahim NR, et al. The effects of physiological biomechanical loading on intradiscal pressure and annulus stress in lumbar spine: a finite element analysis. *J Health Eng*. 2017;8:1-6. doi:[10.1155/2017/9618940](https://doi.org/10.1155/2017/9618940)
 55. Jaumard NV, Welch WC, Winkelstein BA. Spinal facet joint biomechanics and mechanotransduction in normal, injury and degenerative conditions. *J Biomech Eng*. 2011;133(7):071010. doi:[10.1115/1.4004493](https://doi.org/10.1115/1.4004493)
 56. Riggs BL, Melton LJ III. The prevention and treatment of osteoporosis. *N Engl J Med*. 1995;332(12):767-773.
 57. Kanis JA, Johnell O, Oden A, et al. Long-term risk of osteoporotic fracture in Malmo. *Osteoporos Int*. 2000;11(8):669-674.
 58. Majumdar S, Genant HK, Grampp S, et al. Correlation of trabecular bone structure with age, bone mineral density, and osteoporotic status: in vivo studies in the distal radius using high resolution magnetic resonance imaging. *J Bone Miner Res*. 1997;12(1):111-118.
 59. Zhang L, Yang G, Wu L, Yu B. The biomechanical effects of osteoporosis vertebral augmentation with cancellous bone granules or bone cement on treated and adjacent non-treated vertebral bodies: a finite element evaluation. *Clin Biomech (Bristol, Avon)*. 2010;25(2):166-172. doi:[10.1016/j.clinbiomech.2009.10.006](https://doi.org/10.1016/j.clinbiomech.2009.10.006)
 60. Kurutz M, Oroszvary L. Finite element analysis of weightbath hydro-traction treatment of degenerated lumbar spine segments in elastic phase. *J Biomech*. 2010;43(3):433-441.
 61. Mondal S, Ghosh R. Experimental and finite element investigation of total ankle replacement: a review of literature and recommendations. *J Orthop*. 2020;18:41-49. doi:[10.1016/j.jor.2019.09.019](https://doi.org/10.1016/j.jor.2019.09.019)
 62. Mondal S, Ghosh R. Bone remodelling around the tibia due to total ankle replacement: effects of implant material and implant-bone interfacial conditions. *Comput Methods Biomech Biomed Engin*. 2019;22:1247-1257. doi:[10.1080/10255842.2019.1661385](https://doi.org/10.1080/10255842.2019.1661385)
 63. Zhang X, Comellas AP, Regan EA, et al. Quantitative CT-based methods for bone microstructural measures and their relationships with vertebral fractures in a pilot study on smokers. *JBMR Plus*. 2021;5(5):e10484. doi:[10.1002/jbm4.10484](https://doi.org/10.1002/jbm4.10484)
 64. Sollmann N, Rayudu NM, Yeung LY, et al. MDCT-based finite element analyses: are measurements at the lumbar spine associated with the biomechanical strength of functional spinal units of incidental osteoporotic fractures along the thoracolumbar spine? *Diagnostics (Basel)*. 2021;11(3):455. doi:[10.3390/diagnostics11030455](https://doi.org/10.3390/diagnostics11030455)
 65. Valentini A, Trebeschi S, Kaesmacher J, et al. Opportunistic osteoporosis screening in multi-detector CT images via local classification of textures. *Osteoporos Int*. 2019;30:1275-1285. doi:[10.1007/s00198-019-04910-1](https://doi.org/10.1007/s00198-019-04910-1)
 66. Matsuura Y, Giambini H, Ogawa Y, et al. Specimen-specific nonlinear finite element modeling to predict vertebrae fracture loads after vertebroplasty. *Spine*. 2014;39(22):1291-1296. doi:[10.1097/BRS.0000000000000540](https://doi.org/10.1097/BRS.0000000000000540)
 67. Firouzabad A, Arjmand N, Pan F, et al. Sex-dependent estimation of spinal loads during static manual material handling activities—combined in vivo and in silico analyses. *Front Bioeng Biotechnol*. 2021;9:1-14. doi:[10.3389/fbioe.2021.750862](https://doi.org/10.3389/fbioe.2021.750862)
 68. Lee NN, Salzer E, Bach FC, et al. A comprehensive tool box for large animal studies of intervertebral disc degeneration. *JOR Spine*. 2021;4(2):1162. doi:[10.1002/jsp2.1162](https://doi.org/10.1002/jsp2.1162)
 69. Morgan EF, Unnikrisnan GU, Hussein AI. Bone mechanical properties in healthy and diseased states. *Annu Rev Biomed Eng*. 2018;20:119-143. doi:[10.1146/annurev-bioeng-062117-121139](https://doi.org/10.1146/annurev-bioeng-062117-121139)
 70. Oftadeh R, Perez-Viloria M, Villa-Camacho JC, Vaziri A, Nazarian A. Biomechanics and mechanobiology of trabecular bone: a review. *J Biomech Eng*. 2015;137(1):0108021-01080215. doi:[10.1115/1.4029176](https://doi.org/10.1115/1.4029176)
 71. Xu M, Yang J, Lieberman IH, Haddas R. Lumbar spine finite element model for healthy subjects: development and validation. *Comput Methods Biomech Biomed Engin*. 2017;20(1):1-15. doi:[10.1080/10255842.2016.1193596](https://doi.org/10.1080/10255842.2016.1193596)
 72. Nakashima D, Kanchiku T, Nishida N, et al. Finite element analysis of compression fractures at the thoracolumbar junction using models constructed from medical images. *Exp Ther Med*. 2018;15(4):3225-3230. doi:[10.3892/etm.2018.5848](https://doi.org/10.3892/etm.2018.5848)
 73. Lu H, Zhang Q, Ding F, Wu Q, Liu R. Establishment and validation of a T12-L2 3D finite element model for thoracolumbar segments. *Am J Transl Res*. 2022;14(3):1606-1615. <https://www.ncbi.nlm.nih.gov/pmc/articles/PMC8991124/>
 74. Wijayathunga VN, Jones AC, Oakland RJ, Furtado NR, Hall RM, Wilcox RK. Development of specimen-specific finite element models of human vertebrae for the analysis of vertebroplasty. *Proc Inst Mech Eng H*. 2008;222(2):221-228. doi:[10.1243/09544119jeim285](https://doi.org/10.1243/09544119jeim285)
 75. Guo D, Cai J, Zhang S, Zhang L, Feng X. Treating osteoporotic vertebral compression fractures with intraosseous vacuum phenomena using high-viscosity bone cement via bilateral percutaneous vertebroplasty. *Medicine*. 2017;96(14):6549. doi:[10.1097/MD.00000000000006549](https://doi.org/10.1097/MD.00000000000006549)
 76. Mondal S, MacManus DB, Bonatti AF, et al. A computational analysis of a novel therapeutic approach combining an advanced medicinal therapeutic device and a fracture fixation assembly for the treatment of osteoporotic fractures: effects of physiological loading, interface conditions, and fracture fixation materials. *Med Eng Phys*. 2023;114:103967. doi:[10.1016/j.medengphy.2023.103967](https://doi.org/10.1016/j.medengphy.2023.103967)
 77. Kontogianni G-I, Loukelis K, Bonatti AF, et al. Effect of uniaxial compression frequency on osteogenic cell responses in dynamic 3D cultures. *Bioengineering*. 2023;10(5):532. doi:[10.3390/bioengineering10050532](https://doi.org/10.3390/bioengineering10050532)
 78. Frantsuzov R, Mondal S, Walsh CM, Reynolds JP, Dooley D, MacManus DB. A finite element model of contusion spinal cord injury in rodents. *J Mech Behav Biomed Mater*. 2023;142:105856. doi:[10.1016/j.jmbbm.2023.105856](https://doi.org/10.1016/j.jmbbm.2023.105856)
 79. Malandrino A, Noailly J, Lacroix D. Regional annulus fibre orientations used as a tool for the calibration of lumbar intervertebral disc finite element models. *Comput Methods Biomech Biomed Engin*. 2013;16(9):923-928.

SUPPORTING INFORMATION

Additional supporting information can be found online in the Supporting Information section at the end of this article.

How to cite this article: Mondal S, MacManus DB, Banche-Niclot F, et al. Finite element analysis of vertebroplasty in the osteoporotic T11-L1 vertebral body: Effects of bone cement formulation. *J Biomed Mater Res*. 2024;112(1):e35359. doi:[10.1002/jbm.b.35359](https://doi.org/10.1002/jbm.b.35359)